Journal of Materials Chemistry A

PAPER

View Article Online
View Journal | View Issue

Cite this: J. Mater. Chem. A, 2015, 3, 19483

A global view of the phase transitions of SnO_2 in rechargeable batteries based on results of high throughput calculations

Yingchun Cheng,[a] Anmin Nie,[b] Li-Yong Gan,[a] Qingyun Zhang[a] and Udo Schwingenschlögl*[a]

Received 13th May 2015
Accepted 10th August 2015

DOI: 10.1039/c5ta03521j

www.rsc.org/MaterialsA

Lithium, sodium and magnesium have attracted wide attention as potential ions for rechargeable batteries. The Materials Project database of high throughput first principles calculations is used to investigate the phase transitions of SnO_2 during ion intercalation and extraction. Various intermediate phases are predicted to be formed during the first intercalation, whereas in later cycles other intermediate phases are encountered. The volume expansions after intercalation and extraction are analyzed. We show that different lithium and sodium oxide products found in recent experiments are due to different oxygen chemical potentials.

Introduction

Lithium ion batteries are key components in current energy conversion and storage technologies because of their high energy density and long cycle life. However, the ever-growing need for high-capacity storage in applications ranging from portable electronic devices and electric vehicles to green energy requires new battery concepts. Recently, sodium[1–3] and magnesium[4] ion batteries have attracted a lot of interest because of limited lithium reserves and the associated high costs. Alternative active anodes, such as SnO_2, are extensively investigated both experimentally and theoretically with respect to the intercalation, conversion, and alloying mechanisms.[5–13] In this context, SnO_2 possesses a low reaction potential and high theoretical capacity, being cheap and environmentally friendly.[11–16] Due to the relatively short history of SnO_2 based batteries, however, fundamental understanding of the reaction mechanism is missing. Experimentally, the reaction products can be investigated with respect to their short- and long-range atomic structures by X-ray, neutron, and electron diffraction, as well as by nuclear magnetic resonance and other methods.[9–13] *In situ* observation of ion intercalation and extraction by transmission electron microscopy (TEM) has provided atomic scale insight into the reaction dynamics,[9,15–25] whereas theoretical transition barriers and the mechanical failure mechanism have been investigated by first principles calculations.[15–18] Yet, the understanding of the phase transitions in batteries based on SnO_2 is far from complete.

Using the Inorganic Crystal Structure Database,[26] the total energies and electronic structures of a large number of compounds have been determined by the Materials Project[27] and AFLOWLIB consortium[28] by high throughput schemes, making it possible to screen for specific properties[29] and new materials.[30,31] In this work, we demonstrate that the results of high throughput calculations can be used to construct phase diagrams by analyzing the relative thermodynamic stability of different phases using a free energy model.[27,32,33] This allows us to clarify the phase transitions of SnO_2 in Li/Na/Mg ion batteries and particularly to identify intermediate phases, which is key for understanding the battery processes.

Results and discussion

The high throughput data forming the basis of our investigation are taken from the Materials Project database and were obtained by density functional theory as implemented in the Vienna *Ab initio* Simulation Package,[34] using the generalized gradient approximation without and with the onsite Coulomb interaction.[35] The calculations took into account spin-polarization and employed an energy cutoff of 520 eV. The number of points in the k-mesh was set to 1000 divided by the number of atoms in the unit cell. The Gibbs free energy is defined as $G(P, T) = U + PV - TS$, where U, P, V, T, and S are the internal energy, pressure, volume, temperature, and entropy, respectively. In the alkali battery reactions, no gas phase reactants or products are involved and surfaces effects of the electrodes are not considered, so that $P = 0$ GPa and $T = 0$ K are valid approximations.[32,36–42] Therefore, G is given by the internal energy, which corresponds to the total energy of density functional theory.

[a]Department of Materials Science and Engineering, King Abdullah University of Science & Technology, Thuwal, 23955-6900, Kingdom of Saudi Arabia. E-mail: udo.schwingenschlogl@kaust.edu.sa

[b]Department of Mechanical Engineering-Engineering Mechanics, Michigan Technological University, 1400 Townsend Dive, Houghton, Michigan 49931, USA

We used the total energies E_i (per atom) of the involved elements as the reference to define the formation energy $E = (E_{tot} - \sum N_i E_i)/\sum N_i$ of a compound, where E_{tot} is the total energy of the compound and N_i is the amount of atoms in the compound. The structures of bulk lithium, sodium, and magnesium are shown in Fig. 1(a)–(c), respectively. It has been recently found that the reaction product after several cycles of lithiation and delithiation of β-Sn, SnS, and SnO_2 contains a mixture of β-Sn and α-Sn,[34] which are the two Sn polymorphs at ambient pressure. α-Sn (Fig. 1(d)) is stable at temperatures below 13.2 °C and β-Sn (Fig. 1(e)) at temperatures up to 232 °C. We note that cubic α-Sn is favored at small sizes.[9] Sn nanostructures as a function of temperature and size have been investigated recently in ref. 38. The phase diagram of α-Sn, O, and Li/Na/Mg is shown in Fig. 2 including all stable compounds found in high throughput calculations.[27,28] The color indicates the formation energy per atom (E).

It has been conjectured[15] that the first step of the lithiation process is the insertion of Li^+ into the SnO_2 lattice: $SnO_2 + xLi^+ + xe^- \leftrightarrow Li_xSnO_2$. However, what is the detailed phase evolution? The first lithiation line in Fig. 2(a) shows that there exist two lithium tin oxides, Li_2SnO_3 and Li_8SnO_6, see Fig. 3(c) and (d), which have not been characterized experimentally so far.

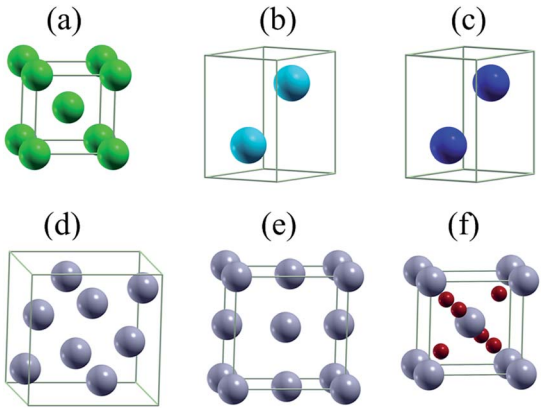

Fig. 1 Unit cells of (a) Li, (b) Na, (c) Mg, (d) α-Sn, (e) β-Sn, and (f) SnO_2. Green, cyan, blue, gray, and red balls represent Li, Na, Mg, Sn, and O atoms.

Li_2SnO_3 is obtained before Li_8SnO_6. Meanwhile, Sn and Li_xSn are formed by means of irreversible conversion of SnO_2 into Sn and lithium oxide: $SnO_2 + 4Li^+ + 4e^- \rightarrow 2Li_2O + Sn$. Finally, there is a reversible alloying reaction: $Sn + xLi^+ + xe^- \leftrightarrow Li_xSn$. All encountered structures are shown in Fig. 3. For sodiation there exist three intermediate phases ($Na_4Sn_3O_8$, Na_4SnO_4, and Na_4SnO_3), see Fig. 4. Theoretically, all mentioned phases can form in Li/Na ion batteries, whereas experimentally it is challenging to identify them by conventional techniques, such as Raman spectroscopy and X-ray diffraction. However, identification can be achieved by *in situ* TEM, though the lithiation/sodiation front is tiny and the process is fast.[15–18]

According to the phase diagram in Fig. 2(a), the final lithiation products are Li_2O and $Li_{17}Sn_4$. The voltage required for the initial lithiation from SnO_2 to Li_2SnO_3 ranges from 1.93 to 1.16 eV for different byproducts, see Table 1. The values are obtained as negative ratios of the change in G and the number of alkali atoms transferred.[43] It is known that Sn nanoparticles form during the first lithiation,[15] while Li_xSn forms without Sn nanoparticles using $LiCoO_2$ as the cathode and a liquid-based electrolyte.[18] The different lithiation products can be attributed to the different experimental setups. The voltage for the second lithiation from Li_2SnO_3 to Li_8SnO_6 is lower as compared to that for the initial lithiation. For lithiation to Li_2O, the voltage ranges from 0.82 to 1.12 eV. We found that the final product is $Li_{17}Sn_4$. During delithiation, Li_2O is assumed to be transformed into Li_2O_2 and $Li_{17}Sn_4$ into Sn. While a transformation from $Li_{17}Sn_4$ to Sn has already been reported,[15] transformation from Li_2O to Li_2O_2 has not been observed yet. The absence of Li_2O_2 is explained by the fact that it will oxidize Li_xSn and Sn to transfer to Li_2O. Therefore, Li_2O is always present. The intermediate phases in later cycles (Li_7Sn_2, $Li_{13}Sn_5$, and LiSn) are different from those during the first lithiation. The voltage profile of Li_nSn shown in Fig. 5(a) is fully consistent with a previous report.[43] Moreover, the reversibility of the Li–Sn alloying process agrees with the cycling behavior observed in ref. 6 for SnO_2 anodes and the formation of Li_2O explains that experimentally the capacity of the battery is reduced after the first cycle.[6,8]

For the first sodiation we found the products Na_2O and $Na_{15}Sn_4$, as identified earlier.[17] According to Fig. 2(b), there are three intermediate phases ($Na_4Sn_3O_8$, Na_4SnO_4, and Na_4SnO_3),

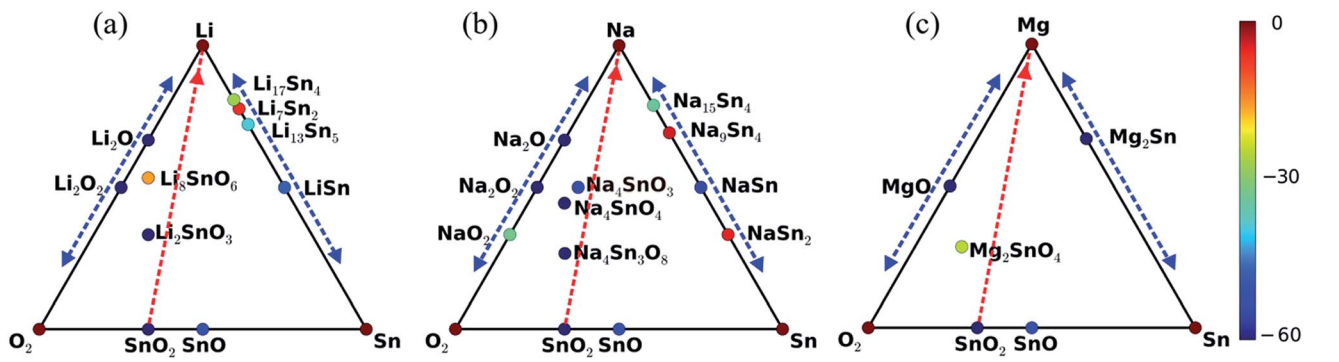

Fig. 2 (a) Li, Sn, O_2, (b) Na, Sn, O_2, and (c) Mg, Sn, O_2 phase diagrams. Circles indicate stable compounds and the colors refer to the formation energy per atom (meV). The red arrow stands for the first intercalation, while the blue arrows represent the following intercalations/extractions.

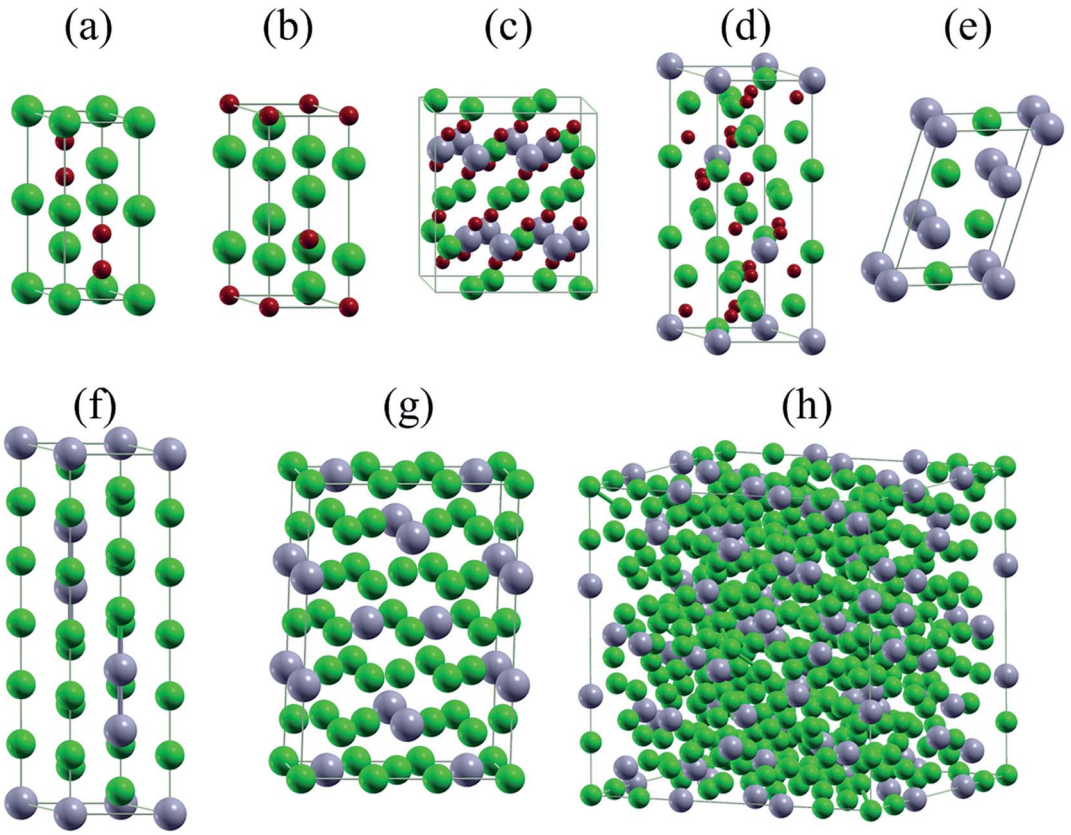

Fig. 3 Unit cells of (a) Li_2O_2, (b) LiO_2, (c) Li_2SnO_3, (d) Li_8SnO_6, (e) LiSn, (f) $Li_{13}Sn_5$, (g) Li_7Sn_2, and (h) $Li_{17}Sn_4$. Green, gray, and red balls represent Li, Sn, and O atoms.

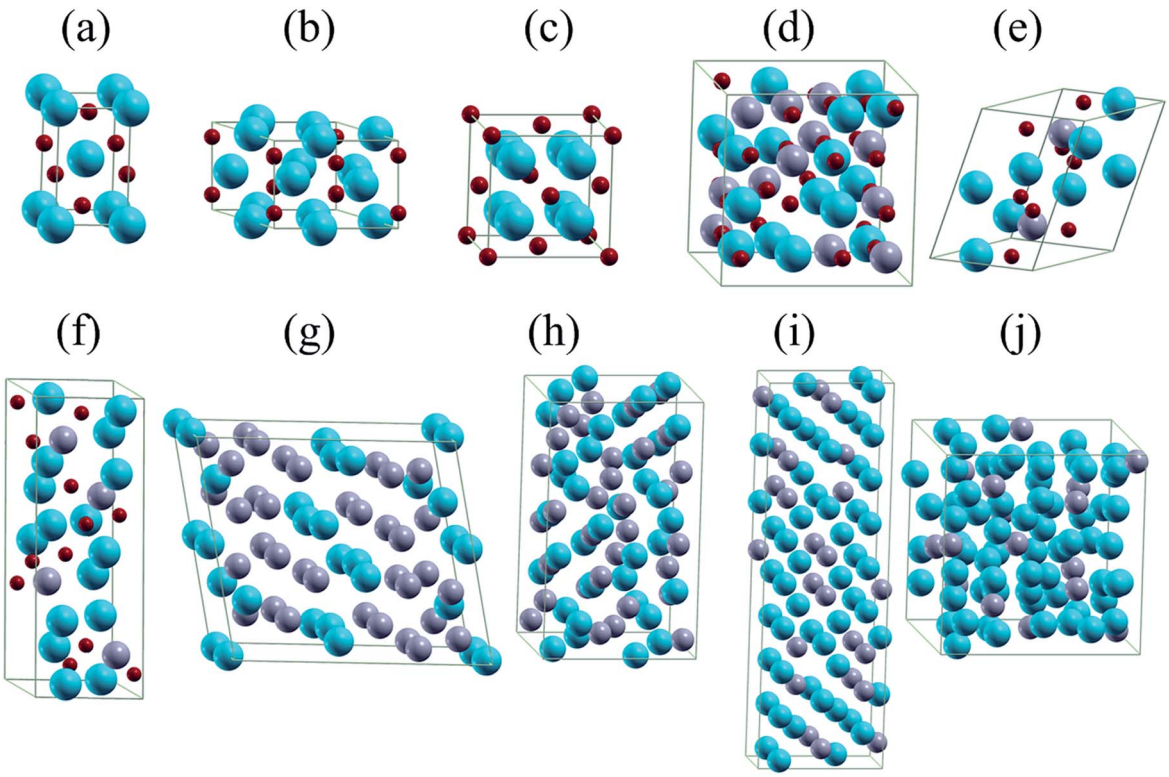

Fig. 4 Unit cells of (a) NaO_2, (b) Na_2O_2, (c) Na_2O, (d) $Na_4Sn_3O_8$, (e) Na_4SnO_4, (f) Na_4SnO_3, (g) $NaSn_2$, (h) NaSn, (i) Na_9Sn_4, and (j) $Na_{15}Sn_4$. Cyan, gray, and red balls represent Na, Sn, and O atoms.

Table 1 Voltage for different reaction paths for lithiation

Reaction	Voltage (eV)
$4Li + 3SnO_2 \rightarrow 2Li_2SnO_3 + Sn$	1.93
$3Li + 3SnO_2 \rightarrow 2Li_2SnO_3 + LiSn$	1.68
$33Li + 15SnO_2 \rightarrow 10Li_2SnO_3 + Li_{13}Sn_5$	1.39
$11Li + 6SnO_2 \rightarrow 4Li_2SnO_3 + Li_7Sn_2$	1.26
$35Li + 12SnO_2 \rightarrow 8Li_2SnO_3 + Li_{17}Sn_4$	1.16
$4Li + 2Li_2SnO_3 \rightarrow Li_8SnO_6 + Sn$	1.36
$3Li + 2Li_2SnO_3 \rightarrow Li_8SnO_6 + LiSn$	1.22
$33Li + 10Li_2SnO_3 \rightarrow 5Li_8SnO_6 + Li_{13}Sn_5$	1.05
$15Li + 4Li_2SnO_3 \rightarrow 2Li_8SnO_6 + Li_7Sn_2$	0.95
$33Li + 8Li_2SnO_3 \rightarrow 4Li_8SnO_6 + Li_{17}Sn_4$	0.88
$3Li + 5Li_8SnO_6 \rightarrow 15Li_2O_2 + Li_{13}Sn_5$	−16.06
$3Li + 2Li_8SnO_6 \rightarrow 6Li_2O_2 + Li_7Sn_2$	−6.27
$9Li + 4Li_8SnO_6 \rightarrow 12Li_2O_2 + Li_{17}Sn_4$	−4.12
$5Li + Li_8SnO_6 \rightarrow 6Li_2O + LiSn$	1.12
$33Li + 5Li_8SnO_6 \rightarrow 30Li_2O + Li_{13}Sn_5$	0.97
$5Li + 2Li_8SnO_6 \rightarrow 12Li_2O + Li_7Sn_2$	0.89
$33Li + 4Li_8SnO_6 \rightarrow 24Li_2O + Li_{17}Sn_4$	0.82

Table 2 Voltage for different reaction paths for sodiation

Reaction	Voltage (eV)
$4Na + 4SnO_2 \rightarrow Na_4Sn_3O_8 + Sn$	1.45
$9Na + 8SnO_2 \rightarrow 2Na_4Sn_3O_8 + NaSn_2$	1.34
$5Na + 4SnO_2 \rightarrow Na_4Sn_3O_8 + NaSn$	1.25
$25Na + 16SnO_2 \rightarrow 4Na_4Sn_3O_8 + Na_9Sn_4$	1.02
$31Na + 16SnO_2 \rightarrow 4Na_4Sn_3O_8 + Na_{15}Sn_4$	0.85
$4Na + Na_4Sn_3O_8 \rightarrow 2Na_4SnO_4 + Sn$	0.65
$9Na + 2Na_4Sn_3O_8 \rightarrow 4Na_4SnO_4 + NaSn_2$	0.63
$5Na + Na_4Sn_3O_8 \rightarrow 2Na_4SnO_4 + NaSn$	0.61
$25Na + 4Na_4Sn_3O_8 \rightarrow 8Na_4SnO_4 + Na_9Sn_4$	0.52
$31Na + 4Na_4Sn_3O_8 \rightarrow 8Na_4SnO_4 + Na_{15}Sn_4$	0.44
$23Na + 4Na_4SnO_3 \rightarrow 12Na_2O + Na_{15}Sn_4$	0.08
$11Na + 4Na_4SnO_3 \rightarrow 6Na_2O_2 + Na_{15}Sn_4$	−1.47
$5Na + 4Na_4SnO_3 \rightarrow 6NaO_2 + Na_{15}Sn_4$	−5.50
$17Na + 4Na_4SnO_3 \rightarrow 12Na_2O + Na_9Sn_4$	0.08
$5Na + 4Na_4SnO_3 \rightarrow 6Na_2O_2 + Na_9Sn_4$	−3.36
$3Na + Na_4SnO_3 \rightarrow 3Na_2O + NaSn$	0.05
$5Na + 2Na_4SnO_3 \rightarrow 6Na_2O + NaSn_2$	−0.03
$2Na + Na_4SnO_3 \rightarrow 3Na_2O + Sn$	−0.15

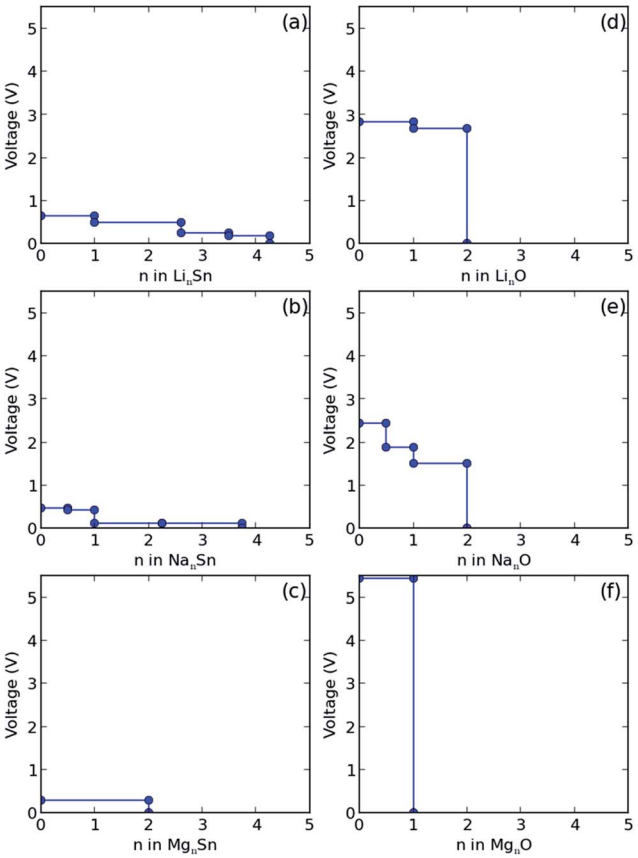

Fig. 5 Voltage profiles of (a) Li$_n$Sn, (b) Na$_n$Sn, (c) Mg$_n$Sn, (d) Li$_n$O, (e) Na$_n$O, and (f) Mg$_n$O.

which have not been observed so far, see the structures in Fig. 4. The voltage required for the first sodiation turns out to be lower than that for the first lithiation (Tables 1 and 2). The lower voltages indicate that sodiation is slower than lithiation, as found earlier for SnO_2,[16–18] which is supported by the higher transition barrier of Na as compared to that of Li. Fig. 2(b) shows that the desodiation products are Na_2O and Sn, as previously identified by TEM.[17] There are Na_2O_2 as well as Na_9Sn_4, NaSn, and $NaSn_2$ intermediate phases and the voltage profile of Na$_n$Sn in Fig. 5(b) is consistent with that reported in the literature.[1]

Instead of Li_2O, Li–O_2 cell experiments found Li_2O_2 as the product by Fourier transform infrared spectroscopy and surface enhanced Raman spectroscopy.[44–46] Though there are reports about the formation of lithium superoxide (LiO_2) in the cell, LiO_2 is unstable and will disproportionate into Li_2O_2 and O_2.[46] Therefore, only Li_2O_2 and Li_2O appear in Fig. 3(a). According to the phase diagram in Fig. 2(b), there are three sodium oxide polymorphs (NaO_2, NaO, and Na_2O), for which the structures are displayed in Fig. 4(a)–(c). *In situ* TEM of sodiation of SnO_2 nanowires found Na_2O as the product,[17] whereas crystalline sodium superoxide (NaO_2) was reported recently for a Na–O_2 cell.[47] The different alkali oxide products after intercalation can be attributed to the oxygen poor environment in the TEM experiments (high vacuum) and the oxygen rich environment in the Li/Na–O_2 cell. Voltage profiles of the Li–O_2 and Na–O_2 cells are shown in Fig. 5(d) and (e), respectively. The voltage for the formation of Li_2O_2 (2.8 eV) is consistent with the experimental value of 2.6 eV,[46,47] whereas that for the formation of NaO_2 (2.4 eV) exceeds the experimental value of 1.8 eV substantially.[47]

Being an additional parameter of the ion battery performance, a large volume expansion indicates the high capacity of the anode but at the same time induces much damage. Since by ion intercalation into SnO_2 the volume will change, we studied the ratio $V_{products}/V_{SnO_2}$, where $V_{products}$ is the total volume of the products and V_{SnO_2} is that of SnO_2. We obtained values of 3.8/6.1 for Li/Na, which suggests a higher capacity for Na than for Li. For the extraction process, the result is 1.9/2.0 for Li/Na and thus more than 1, which indicates irreversibility for both Na and Li. The volume expansion after the first sodiation of a SnO_2 nanowire is 4.7,[19] which is less than the theoretical value, and 2.6 after the first desodiation, which exceeds the theoretical value of 2.0.

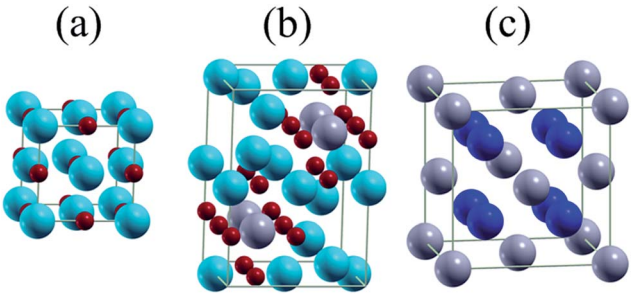

Fig. 6 Unit cells of (a) MgO, (b) Mg_2SnO_4, and (c) Mg_2Sn. Blue, gray, and red balls represent Mg, Sn, and O atoms.

Table 3 Voltage for different reaction paths for magnesiation

Reaction	Voltage (eV)
$2Mg + 2SnO_2 \rightarrow Mg_2SnO_4 + Sn$	3.04
$4Mg + 2SnO_2 \rightarrow Mg_2SnO_4 + Mg_2Sn$	1.66
$2Mg + Mg_2SnO_4 \rightarrow 4MgO + Sn$	2.87
$4Mg + Mg_2SnO_4 \rightarrow 4MgO + Mg_2Sn$	1.58

This discrepancy points to incomplete sodiation and desodiation in the experiment. Moreover, the volume expansion decreases for further sodiation and increases for further desodiation, which suggests the formation of intermediate structures that hinder the cycling and eventually result in failure of batteries. The formation of such structures also could be the origin of observed cracking.[19] During a full cycle, the volume changes by a factor of 2.0 for Li and a larger factor of 3.0 for Na.

According to Fig. 2(c), there is only one intermediate phase for magnesiation (Mg_2SnO_4), see the structure in Fig. 6, and the products are MgO and Mg_2Sn. Because there are no other magnesium oxide phases, it is difficult to transform MgO, see the Mg_nO voltage profile in Fig. 5(f). By comparing Table 3 with Tables 1 and 2 we find that the voltage required for the first magnesiation is much higher than in the cases of lithiation and sodiation. The value of 5.5 eV is much higher than that found for lithiation and sodiation, which implies that SnO_2 is not a suitable anode for magnesium ion batteries. Only one magnesium tin alloy (Mg_2Sn) appears in Fig. 2(c). However, the Mg_nSn voltage is 0.3 eV and thus much lower than the values found for Li_nSn and Na_nSn. Therefore, it is expected that the products of demagnesiation are Sn and MgO. We obtained theoretical volume expansions of 3.1 and 2.0 for magnesiation and demagnesiation, respectively.

While our present study focuses on the phase transitions in the SnO_2 electrode during alkali ion intercalation, typically also the interface between the electrolyte and the electrodes (both cathode and anode) plays an important role in the performance of batteries. For example, it has been demonstrated theoretically that the voltage depends on the surface charge density,[48,49] which can explain differences between experimental values and the voltages calculated for bulk electrodes. Important challenges for the first principles modeling in this area have been reviewed very recently in ref. 50.

Conclusions

Based on the results taken from the Materials Project database of high throughput first principles calculations, we have established the Sn, O, and Li/Na/Mg phase diagram for batteries based on SnO_2. For the first intercalation, we predict intermediate phases (Li_2SnO_3 and Li_8SnO_6 for lithiation, $Na_4Sn_3O_8$, Na_4SnO_4, and Na_4SnO_3 for sodiation, and Mg_2SnO_4 for magnesiation) which so far have not been verified experimentally. After full intercalation SnO_2 is transformed into tin alloys ($Li_{17}Sn_4$, $Na_{15}Sn_4$, and Mg_2Sn) and oxides (Li_2O, Na_2O, and MgO) and after full extraction the products are Sn and oxides (Li_2O_2, NaO_2, and MgO). The volume expansion after Li/Na/Mg intercalation is predicted as 3.8/6.1/3.1 and that after extraction as 1.9/2.1/2.0. Different oxide products found in recent experiments on Li/Na air batteries and in *in situ* TEM on nanowires are attributed to different oxygen chemical potentials in the two experiments. Comparison of different reaction paths allows us to predict that an applied voltage experimentally will have a crucial effect on the final products, which is an important insight because voltage dependent investigations are still strongly limited today. We have demonstrated that the results of high throughput calculations can be used for predicting the phase transitions in batteries and thus pave the way to provide instructions for the development of novel battery concepts.

Acknowledgements

Research reported in this publication was supported by the King Abdullah University of Science and Technology (KAUST).

References

1 V. L. Chevrier and G. Ceder, Challenges for Na-Ion Negative Electrodes, *J. Electrochem. Soc.*, 2011, **158**, A1011–A1014.
2 V. Palomares, P. Serras, I. Villaluenga, K. B. Hueso, J. Carretero-Gonzalez and T. Rojo, Na-Ion Batteries, Recent Advances and Present Challenges to Become Low Cost Energy Storage Systems, *Energy Environ. Sci.*, 2012, **5**, 5884–5901.
3 N. Yabuuchi, K. Kubota, M. Dahbi and S. Komaba, Research Development on Sodium-Ion Batteries, *Chem. Rev.*, 2014, **114**, 11636–11682.
4 H. D. Yoo, I. Shterenberg, Y. Gofer, G. Gershinsky, N. Pour and D. Aurbach, Mg Rechargeable Batteries: an On-Going Challenge, *Energy Environ. Sci.*, 2013, **6**, 2265–2279.
5 J. Yang, M. Winter and J. O. Besenhard, Small Particle Size Multiphase Li-alloy Anodes for Lithium-ion-batteries, *Solid State Ionics*, 1996, **90**, 281–287.
6 I. A. Courtney and J. R. Dahn, Electrochemical and *In Situ* X-ray Diffraction Studies of The Reaction of Lithium with Tin Oxide Composites, *J. Electrochem. Soc.*, 1997, **144**, 2045–2052.
7 Y. Idota, T. Kubota, A. Matsufuji, Y. Maekawa and T. Miyasaka, Tin-based Amorphous Oxide: A High-capacity Lithium-ion-storage Material, *Science*, 1997, **276**, 1395–1397.

8 T. Brousse, R. Retoux, U. Herterich and D. M. Schleich, Thin-film Crystalline SnO_2-lithium Electrodes, *J. Electrochem. Soc.*, 1998, **145**, 1–4.

9 C. Kim, M. Noh, M. Choi, J. Cho and B. Park, Critical Size of a Nano SnO_2 Electrode for Li-secondary Battery, *Chem. Mater.*, 2005, **17**, 3297–3301.

10 Y. Wang, D. W. Su, C. Y. Wang and G. X. Wang, SnO_2@MWCNT Nanocomposite as a High Capacity Anode Material for Sodium-Ion Batteries, *Electrochem. Commun.*, 2013, **29**, 8–11.

11 D. W. Su, H. J. Ahn and G. X. Wang, SnO_2@Graphene Nanocomposites as Anode Materials for Na-ion Batteries with Superior Electrochemical Performance, *Chem. Commun.*, 2013, **49**, 3131–3133.

12 T. Xiao, Y. W. Tang, Z. Y. Jia and S. L. Feng, Synthesis of SnO_2/Mg_2SnO_4 Nanoparticles and Their Electrochemical Performance for Use in Li-ion Battery Electrodes, *Electrochim. Acta*, 2009, **54**, 2396–2401.

13 Y. X. Wang, Y. G. Lim, M. S. Park, S. L. Chou, J. H. Kim, H. K. Liu, *et al.* Ultrafine SnO_2 Nanoparticle Loading onto Reduced Graphene Oxide as Anodes for Sodium-Ion Batteries with Superior Rate and Cycling Performances, *J. Mater. Chem. A*, 2014, **2**, 529–534.

14 H. Zheng, J. B. Wang, J. Y. Huang, A. J. Cao and S. X. Mao, *In Situ* Visualization of Birth and Annihilation of Grain Boundaries in an Au Nanocrystal, *Phys. Rev. Lett.*, 2012, **109**, 225501.

15 A. M. Nie, L. Y. Gan, Y. C. Cheng, H. Asayesh-Ardakani, Q. Q. Li, C. Z. Dong, *et al.* Atomic-Scale Observation of Lithiation Reaction Front in Nanoscale SnO_2 Materials, *ACS Nano*, 2013, **7**, 6203–6211.

16 J. Y. Huang, L. Zhong, C. M. Wang, J. P. Sullivan, W. Xu, L. Q. Zhang, *et al. In Situ* Observation of the Electrochemical Lithiation of a Single SnO_2 Nanowire Electrode, *Science*, 2010, **330**, 1515–1520.

17 M. Gu, A. Kushima, Y. Y. Shao, J. G. Zhang, J. Liu, N. D. Browning, *et al.* Probing the Failure Mechanism of SnO_2 Nanowires for Sodium-Ion Batteries, *Nano Lett.*, 2013, **13**, 5203–5211.

18 C. M. Wang, W. Xu, J. Liu, J. G. Zhang, L. V. Saraf, B. W. Arey, *et al. In Situ* Transmission Electron Microscopy Observation of Microstructure and Phase Evolution in a SnO_2 Nanowire during Lithium Intercalation, *Nano Lett.*, 2011, **11**, 1874–1880.

19 M. Gu, Y. Li, X. L. Li, S. Y. Hu, X. W. Zhang, W. Xu, *et al. In Situ* TEM Study of Lithiation Behavior of Silicon Nanoparticles Attached to and Embedded in a Carbon Matrix, *ACS Nano*, 2012, **6**, 8439–8447.

20 N. Liu, H. Wu, M. T. McDowell, Y. Yao, C. M. Wang and Y. Cui, A Yolk-Shell Design for Stabilized and Scalable Li-Ion Battery Alloy Anodes, *Nano Lett.*, 2012, **12**, 3315–3321.

21 X. H. Liu, Y. Liu, A. Kushima, S. L. Zhang, T. Zhu, J. Li, *et al. In Situ* TEM Experiments of Electrochemical Lithiation and Delithiation of Individual Nanostructures, *Adv. Eng. Mater.*, 2012, **2**, 722–741.

22 X. H. Liu, J. W. Wang, S. Huang, F. F. Fan, X. Huang, Y. Liu, *et al. In Situ* Atomic-Scale Imaging of Electrochemical Lithiation in Silicon, *Nat. Nanotechnol.*, 2012, **7**, 749–756.

23 X. H. Liu, J. W. Wang, Y. Liu, H. Zheng, A. Kushima, S. Huang, *et al. In situ* Transmission Electron Microscopy of Electrochemical Lithiation, Delithiation and Deformation of Individual Graphene Nanoribbons, *Carbon*, 2012, **50**, 3836–3844.

24 X. H. Liu, L. Zhong, S. Huang, S. X. Mao, T. Zhu and J. Y. Huang, Size-Dependent Fracture of Silicon Nanoparticles during Lithiation, *ACS Nano*, 2012, **6**, 1522–1531.

25 H. Yang, S. Huang, X. Huang, F. F. Fan, W. T. Liang, X. H. Liu, *et al.* Orientation-Dependent Interfacial Mobility Governs the Anisotropic Swelling in Lithiated Silicon Nanowires, *Nano Lett.*, 2012, **12**, 1953–1958.

26 G. Bergerhoff, R. Hundt, R. Sievers and I. D. Brown, The Inorganic Crystal-Structure Database, *J. Chem. Inf. Comput. Sci.*, 1983, **23**, 66.

27 A. Jain, G. Hautier, C. J. Moore, S. P. Ong, C. C. Fischer, T. Mueller, *et al.* A High-Throughput Infrastructure For Density Functional Theory Calculations, *Comput. Mater. Sci.*, 2011, **50**, 2295–2310.

28 S. Curtarolo, W. Setyawan, S. D. Wang, J. K. Xue, K. S. Yang, R. H. Taylor, *et al.* AFLOWLIB.ORG: A Distributed Materials Properties Repository From High-Throughput *Ab Initio* Calculations, *Comput. Mater. Sci.*, 2012, **58**, 227–235.

29 S. Curtarolo, G. L. W. Hart, M. B. Nardelli, N. Mingo, S. Sanvito and O. Levy, The High-Throughput Highway to Computational Materials Design, *Nat. Mater.*, 2013, **12**, 191–201.

30 A. N. Kolmogorov and S. Curtarolo, Prediction of Different Crystal Structure Phases in Metal Borides: A Lithium Monoboride Analog to MgB_2, *Phys. Rev. B: Condens. Matter Mater. Phys.*, 2006, **73**, 180501.

31 A. N. Kolmogorov, S. Shah, E. R. Margine, A. F. Bialon, T. Hammerschmidt and R. Drautz, New Superconducting and Semiconducting Fe-B Compounds Predicted with an *Ab Initio* Evolutionary Search, *Phys. Rev. Lett.*, 2010, **105**, 217003.

32 S. P. Ong, L. Wang, B. Kang and G. Ceder, Li-Fe-P-O_2 Phase Diagram from First Principles Calculations, *Chem. Mater.*, 2008, **20**, 1798–1807.

33 S. P. Ong, A. Jain, G. Hautier, B. Kang and G. Ceder, Thermal Stabilities of Delithiated Olivine MPO_4 (M = Fe, Mn) Cathodes Investigated Using First Principles Calculations, *Electrochem. Commun.*, 2010, **12**, 427–430.

34 G. Kresse and J. Furthmüller, Efficient Iterative Schemes for *Ab Initio* Total-Energy Calculations Using a Plane-Wave Basis Set, *Phys. Rev. B: Condens. Matter Mater. Phys.*, 1996, **54**, 11169–11186.

35 A. Jain, G. Hautier, S. P. Ong, C. Moore, C. C. Fischer, K. A. Persson, *et al.* Formation Enthalpies by Mixing GGA and GGA+U calculations, *Phys. Rev. B: Condens. Matter Mater. Phys.*, 2011, **84**, 045115.

36 K. Reuter and M. Scheffler, Composition, Structure, and Stability of RuO_2(110) as a Function of Oxygen Pressure, *Phys. Rev. B: Condens. Matter Mater. Phys.*, 2001, **65**, 035406.
37 K. Reuter and M. Scheffler, First-Principles Atomistic Thermodynamics for Oxidation Catalysis: Surface Phase Diagrams and Catalytically Interesting Regions, *Phys. Rev. Lett.*, 2003, **90**, 046103.
38 N. G. Hörmann, A. Gross and P. Kaghazchi, Semiconductor-Metal Transition Induced by Nanoscale Stabilization, *Phys. Chem. Chem. Phys.*, 2015, **17**, 5569–5573.
39 M. H. Hansen, L. A. Stern, L. G. Feng, J. Rossmeisl and X. L. Hu, Widely Available Active Sites on Ni_2P for Electrochemical Hydrogen Evolution – Insights from First Principles Calculations, *Phys. Chem. Chem. Phys.*, 2015, **17**, 10823–10829.
40 M. Nielsen, M. E. Bjorketun, M. H. Hansen and J. Rossmeisl, Towards First Principles Modeling of Electrochemical Electrode–Electrolyte Interfaces, *Surf. Sci.*, 2015, **631**, 2–7.
41 M. Garcia-Mota, A. Vojvodic, F. Abild-Pedersen and J. K. Norskov, Electronic Origin of the Surface Reactivity of Transition-Metal-Doped TiO_2(110), *J. Phys. Chem. C*, 2013, **117**, 460–465.
42 F. Abild-Pedersen, J. Greeley, F. Studt, J. Rossmeisl, T. R. Munter, P. G. Moses, *et al.* Scaling Properties of Adsorption Energies for Hydrogen-Containing Molecules on Transition-Metal Surfaces, *Phys. Rev. Lett.*, 2007, **99**, 016105.
43 I. A. Courtney, J. S. Tse, O. Mao, J. Hafner and J. R. Dahn, *Ab Initio* Calculation of the Lithium–Tin Voltage Profile, *Phys. Rev. B: Condens. Matter Mater. Phys.*, 1998, **58**, 15583–15588.
44 T. Zhang and H. S. Zhou, A Reversible Long-Life Lithium–Air Battery in Ambient Air, *Nat. Commun.*, 2013, **4**, 1817.
45 Z. Q. Peng, S. A. Freunberger, Y. H. Chen and P. G. Bruce, A Reversible and Higher-Rate Li-O_2 Battery, *Science*, 2012, **337**, 563–566.
46 Z. Q. Peng, S. A. Freunberger, L. J. Hardwick, Y. H. Chen, V. Giordani, F. Barde, *et al.* Oxygen Reactions in a Non-Aqueous Li^+ Electrolyte, *Angew. Chem., Int. Ed.*, 2011, **50**, 6351–6355.
47 P. Hartmann, C. L. Bender, M. Vracar, A. K. Durr, A. Garsuch, J. Janek, *et al.* A Rechargeable Room-Temperature Sodium Superoxide (NaO_2) Battery, *Nat. Mater.*, 2013, **12**, 228–232.
48 K. Leung and C. M. Tenney, Toward First Principles Prediction of Voltage Dependences of Electrolyte/Electrolyte Interfacial Processes in Lithium Ion Batteries, *J. Phys. Chem. C*, 2013, **117**, 24224–24235.
49 K. Leung, Predicting the Voltage Dependence of Interfacial Electrochemical Processes at Lithium-Intercalated Graphite Edge Planes, *Phys. Chem. Chem. Phys.*, 2015, **17**, 1637–1643.
50 N. G. Hörmann, M. Jäckle, F. Gossenberger, T. Roman, K. Forster-Tonigold, M. Naderian, *et al.* Some Challenges in the First-Principles Modeling of Structures and Processes in Electrochemical Energy Storage and Transfer, *J. Power Sources*, 2015, **275**, 531–538.